Analyzing bull's eye structures by a vertical mode expansion method with rotational symmetry

Xun Lu[1] and Ya Yan Lu[1,*]

[1]*Department of Mathematics, City University of Hong Kong, Kowloon, Hong Kong*

compiled: September 23, 2015

A bull's eye structure is a metallic film with a circular subwavelength aperture surrounded by concentric annular grooves. It is an important structure for realizing applications of the extraordinary optical transmission phenomenon. The structure is invariant under rotations about the central axis perpendicular to the film. In this paper, an efficient numerical method is developed for analyzing bull's eye and other structures that consist of different annular regions where the material properties are one-dimensional. The method is a new variant of the recently developed vertical mode expansion method (VMEM) which combines field expansions in one-dimensional eigenmodes with various techniques for solving scalar two-dimensional Helmholtz equations. The method exploits the rotational symmetry by solving the different Fourier components separately. For normal incident waves, the method is particularly efficient, since it is only necessary to solve one Fourier mode. The method is used to analyze bull's eye structures with different configurations. In particular, we found that the normalized transmission coefficient can be larger than 52 for a bull's eye structure with 22 grooves.

OCIS codes: (050.1220) Apertures; (050.2770) Gratings; (050.6624) Subwavelength structures; (050.1755) Computational electromagnetic methods.

http://dx.doi.org/10.1364/XX.99.099999

1. Introduction

In recent years, the extraordinary optical transmission (EOT) phenomenon for subwavelength apertures in metallic films has attracted much attention [1–3]. The bull's eye structures (single subwavelength apertures surrounded by annular grooves) are particularly interesting and have potential applications in nanolithography and data storage, since the transmitted light can have very high intensity and be highly focused [4, 5]. The physical mechanism for light transmission through bull's eye structures has been thoroughly investigated [2, 3, 6, 7]. These studies provide valuable information on choosing some key parameters for bull's eye structures, but rigorous numerical simulations based on solving the full Maxwell's equations are still needed to optimize the performance of bull's eye structures in practical applications [8–11].

Standard computational electromagnetics methods, such as the finite-difference time-domain (FDTD) method and the frequency-domain finite element and boundary element methods, can be used to analyze bull's eye structures. FDTD is time consuming, since a small grid size and a small time step are needed. The finite element method gives rise to a large complex non-Hermitian and indefinite linear system which can be expensive to solve. The boundary element method is rather complicated to implement [12]. Another possibility is to use a modal method, such as the one based on Fourier-Bessel expansions [8] or the Fourier modal method [13–16]. A modal method expands the electromagnetic field in two-dimensional eigenmodes. Unfortunately, a large number of eigenmodes are needed, and these full-vectorial modes are expensive to calculate.

In a recent work [17], we developed a vertical mode expansion method (VMEM) for analyzing the transmission of light through a circular aperture in a metallic film. The method in related to the early works on photonic crystal slabs [18–20]. The basic idea is to divide the structure into different regions where the material properties depend only on the vertical variable z perpendicular to the film, to expand the electromagnetic field in each region, and to match the tangential field components on the vertical boundaries between these regions. Extended versions of the VMEM are applicable to more general cylindrical structures and have been used to analyze metallic nanoparticles on a substrate [21, 22].

In this paper, we develop a special VMEM for structures with a continuous rotational symmetry, and use it to analyze bull's eye structures. The rotational symmetry gives a major simplification to the method, since the field can be expanded in Fourier series of θ (the horizontal angle), and the different Fourier components are completely decoupled and can be solved separately. For a normal incident plane wave, a further significant simplification can be realized, since the only non-zero Fourier components are those corresponding to $\exp(\pm i\theta)$. Using

* Corresponding author: mayylu@cityu.edu.hk

the special VMEM, we analyze bull's eye structures for a few different configurations.

2. Problem formulation

We consider a rotationally symmetric structure with multiple annular regions, where the material properties in each region depend only on the vertical variable z. In a cylindrical coordinate system where a point $\boldsymbol{r}$ is represented by its horizontal radial distance r, horizontal angle θ and height z, we have $0 < r_1 < r_2 < ... < r_L$, such that the three-dimensional (3D) regions S_0, S_l (for $1 \le l < L$) and S_L are given by $r < r_1$, $r_l < r < r_{l+1}$ (for $1 \le l < L$) and $r > r_L$, respectively. Notice that S_l (for $0 \le l \le L$) are 3D regions for all z and all θ. We denote the two-dimensional (2D) cross section of S_l by Ω_l. Let ε and μ be the relative permittivity and the relative permeability, respectively, then

$$\varepsilon = \varepsilon^{(l)}(z), \quad \mu = \mu^{(l)}(z), \quad \boldsymbol{r} \in S_l. \tag{1}$$

It is further assumed that the main part of the structure is restricted in the vertical direction by $0 < z < D$ for some $D > 0$, and the media in the top ($z > D$) and bottom ($z < 0$) are homogeneous with $\varepsilon = \varepsilon_t$, $\mu = \mu_t$ for $z > D$, and $\varepsilon = \varepsilon_b$, $\mu = \mu_b$ for $z < 0$, where ε_t, μ_t, ε_b and μ_b are real positive constants.

In Fig. 1, we show a vertical cross section of a bull's eye

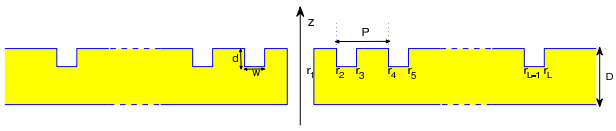

Fig. 1. Schematic representation of bull's eye structure

structure, where r_1 is the radius of the circular hole in the center, r_2 and r_3 are the inner and outer radii of the first groove, r_4 and r_5 are the inner and outer radii of the second groove, etc. The regions given by $r_1 < r < r_2$, $r_3 < r < r_4$, ..., and $r > r_L$ (where L must be an odd integer) correspond to the original metallic film of thickness D. Furthermore, all grooves are assumed to have the same width w ($w = r_3 - r_2 = r_5 - r_4 = ...$) and depth d, and placed periodically in r with period P ($P = r_4 - r_2 = r_5 - r_3 = ...$). Notice that for such a bull's eye structure, there are only three distinct vertical profiles corresponding to the central hole, the original metallic film and the groove.

Our starting point is the frequency-domain Maxwell's equations

$$\nabla \times \mathbf{E} = \mathrm{i}k_0\mu\mathbf{H}, \quad \nabla \times \mathbf{H} = -\mathrm{i}k_0\varepsilon\mathbf{E}, \tag{2}$$

where k_0 is the free space wavenumber, $\mathbf{E}$ is the electric field, and $\mathbf{H}$ is the magnetic field multiplied by the free space impedance. The time dependence is assumed to be $e^{-\mathrm{i}\omega t}$ for an angular frequency ω. In the top homogeneous medium, we specify a plane incident wave with the wave vector $(\alpha, \beta, -\gamma)$, where α and β are real, and $\gamma = (k_0^2\varepsilon_t\mu_t - \alpha^2 - \beta^2)^{1/2}$ is positive.

3. VMEM: basic steps

In contrast to the standard modal method [13–16] which divides the structure into a number of z-invariant layers, VMEM devides the structure into different regions where the material properties depend only on z. For the bull's eye structure shown in Fig. 1, the modal method expands the field in four layers (given by $z < 0$, $0 < z < D - d$, $D - d < z < D$, and $z > D$, respectively), while VMEM expands the field in regions S_l for $0 \le l \le L$.

In [17], a detailed derivation of field expansions used in VMEM is presented. In this section, we outline the basic steps without repeating the details. In region S_l, we first calculate one-dimensional (1D) eigenmodes $\phi_j^{(l,p)}(z)$, where p is the polarization index ($p = e$ for a transverse electric (TE) mode, $p = h$ for a transverse magnetic (TM) mode), j is the mode index, and l is the location index. The related propagation constant is denoted as $\eta_j^{(l,p)}$. The definition of these modes follows that for planar waveguides. Since z is unbounded, it is truncated to a finite interval (z_b, z_t) with perfectly matched layers (PMLs) near the two endpoints. The function $\phi_j^{(l,p)}$ and the constant $\eta_j^{(l,p)}$ satisfy an eigenvalue equation and zero boundary conditions at $z = z_b$ and z_t [17]. Related to the mode $\phi_j^{(l,p)}$ is an unknown 2D function $V_j^{(l,p)}$ (the expansion "coefficient") satisfying the Helmholtz equation

$$\frac{\partial^2 V_j^{(l,p)}}{\partial x^2} + \frac{\partial^2 V_j^{(l,p)}}{\partial y^2} + [\eta_j^{(l,p)}]^2 V_j^{(l,p)} = 0 \quad \text{in} \quad \Omega_l, \tag{3}$$

where Ω_l is the 2D cross section of S_l.

For a hypothetical infinite 1D structure with $\varepsilon = \varepsilon^{(l)}(z)$ and $\mu = \mu^{(l)}(z)$, the incident wave $\{\mathbf{E}^{(i)}, \mathbf{H}^{(i)}\}$ gives rise to a simple 1D solution which we denote as $\{\mathbf{E}^{(l)}, \mathbf{H}^{(l)}\}$. In region S_l, the vertical mode expansions are

$$H_z = H_z^{(l)} + \frac{1}{\mu^{(l)}} \sum_{j=1}^{\infty} [\eta_j^{(l,e)}]^2 \phi_j^{(l,e)} V_j^{(l,e)}, \tag{4}$$

$$E_z = E_z^{(l)} + \frac{1}{\varepsilon^{(l)}} \sum_{j=1}^{\infty} [\eta_j^{(l,h)}]^2 \phi_j^{(l,h)} V_j^{(l,h)}, \tag{5}$$

$$H_\tau = H_\tau^{(l)} + \frac{1}{\mu^{(l)}} \sum_{j=1}^{\infty} \frac{d\phi_j^{(l,e)}}{dz} \frac{\partial V_j^{(l,e)}}{\partial \tau} + \mathrm{i}k_0 \sum_{j=1}^{\infty} \phi_j^{(l,h)} \frac{\partial V_j^{(l,h)}}{\partial \nu}, \tag{6}$$

$$E_\tau = E_\tau^{(l)} + \frac{1}{\varepsilon^{(l)}} \sum_{j=1}^{\infty} \frac{d\phi_j^{(l,h)}}{dz} \frac{\partial V_j^{(l,h)}}{\partial \tau} - \mathrm{i}k_0 \sum_{j=1}^{\infty} \phi_j^{(l,e)} \frac{\partial V_j^{(l,e)}}{\partial \nu}, \tag{7}$$

where $\nu = (\nu_x, \nu_y)$ and $\tau = (-\nu_y, \nu_x)$ are a pair of orthogonal unit vectors in the horizontal plane, H_τ and E_τ

are horizontal components in the τ direction, $\partial/\partial\tau$ and $\partial/\partial\nu$ are directional derivative operators, $H_z^{(l)}$ is the z component of the 1D solution $\mathbf{H}^{(l)}$, etc. The above expansions are derived from the full Maxwell's equations without any approximation, except for a truncation of z with PMLs. In these equations, the functions $V_j^{(l,p)}$ are the unknowns, but they satisfy Eq. (3). More details on Eqs. (3)-(7) are given in [17].

The approach used in [17, 21] is to solve $V_j^{(l,p)}$ on $\partial\Omega_l$ (the boundary of Ω_l). Assuming ν and τ are the unit normal and tangential vectors of $\partial\Omega_l$, we can set up a linear system for all $V_j^{(l,p)}$ on $\partial\Omega_l$ by matching E_z, H_z, E_τ and H_τ on the vertical boundaries between the different regions. The approach used in [22] is to solve all $\partial_\nu V_j^{(l,p)}$ on $\partial\Omega_l$, because it is easier to link $V_j^{(l,p)}$ to $\partial_\nu V_j^{(l,p)}$ (instead of the other way around) by a boundary integral equation. In the next section, we present an efficient procedure to calculate $V_j^{(l,p)}$ for structures with a continuous rotational symmetry.

4. VMEM: rotational symmetry

The structures described in Section 2 are invariant under rotations around the z axis. If the electromagnetic field is expanded in Fourier series of θ, then the different Fourier modes are completely decoupled and they can be solved independently. Since $V_j^{(l,p)}$ satisfies Helmholtz equation (3) in Ω_l, it can be expanded in cylindrical waves. For $1 \le l < L$, we have

$$V_j^{(l,p)} = \sum_{m=-\infty}^{\infty} \left[a_{j,m}^{(l,p)} \frac{H_m^{(1)}(\eta_j^{(l,p)} r)}{H_m^{(1)}(\eta_j^{(l,p)} r_l)} + b_{j,m}^{(l,p)} \frac{H_m^{(2)}(\eta_j^{(l,p)} r)}{H_m^{(1)}(\eta_j^{(l,p)} r_{l+1})} \right] e^{\mathrm{i}m\theta}, \quad r_l < r < r_{l+1}, \quad (8)$$

where $H_m^{(1)}$ and $H_m^{(2)}$ are mth order Hankel functions of first and second kinds. In Ω_0 and Ω_L, we have

$$V_j^{(0,p)} = \sum_{m=-\infty}^{\infty} b_{j,m}^{(0,p)} \frac{J_m(\eta_j^{(l,p)} r)}{J_m(\eta_j^{(l,p)} r_1)} e^{\mathrm{i}m\theta}, \ r < r_1, \quad (9)$$

$$V_j^{(L,p)} = \sum_{m=-\infty}^{\infty} a_{j,m}^{(L,p)} \frac{H_m^{(1)}(\eta_j^{(L,p)} r)}{H_m^{(1)}(\eta_j^{(L,p)} r_L)} e^{\mathrm{i}m\theta}, \ r > r_L, \quad (10)$$

where J_m is the mth order Bessel function of the first kind. On the circle $r = r_l$, the unit normal and tangential vectors are $\nu = (\cos\theta, \sin\theta)$ and $\tau = (-\sin\theta, \cos\theta)$. Therefore, H_τ and E_τ are just the θ components of the electromagnetic field (usually denoted as H_θ and E_θ).

For each fixed m, we can set up a linear system

$$\mathbf{A}_m \boldsymbol{x}_m = \boldsymbol{c}_m, \quad (11)$$

where

$$\boldsymbol{x}_m = \begin{bmatrix} \boldsymbol{b}_m^{(0)} \\ \boldsymbol{a}_m^{(1)} \\ \boldsymbol{b}_m^{(1)} \\ \boldsymbol{a}_m^{(2)} \\ \vdots \\ \boldsymbol{a}_m^{(L)} \end{bmatrix}, \ \boldsymbol{a}_m^{(l)} = \begin{bmatrix} a_{1,m}^{(l,e)} \\ a_{2,m}^{(l,e)} \\ \vdots \\ a_{1,m}^{(l,h)} \\ a_{2,m}^{(l,h)} \\ \vdots \end{bmatrix}, \ \boldsymbol{b}_m^{(l)} = \begin{bmatrix} b_{1,m}^{(l,e)} \\ b_{2,m}^{(l,e)} \\ \vdots \\ b_{1,m}^{(l,h)} \\ b_{2,m}^{(l,h)} \\ \vdots \end{bmatrix}. \quad (12)$$

Equation (11) comes from the continuity of H_z, E_z, H_τ and E_τ at $r = r_l$ for $1 \le l \le L$. In the fully discretized version, the variable z is discretized by N_z points z_n for $1 \le n \le N_z$, a numerical method (the pseudospectral method) is used to calculate the vertical modes $\phi_j^{(l,p)}$. We obtain N_z numerical TE modes and N_z numerical TM modes, then the index j ranges from 1 to N_z, the vectors $\boldsymbol{a}_m^{(l)}$ and $\boldsymbol{b}_m^{(l)}$ are column vectors of length $2N_z$, and $\mathbf{A}_m$ is a $(4LN_z) \times (4LN_z)$ matrix. To obtain Eq. (11), we match the mth Fourier coefficients of H_z, E_z, H_τ and E_τ at r_l $(1 \le l \le L)$ and z_n $(1 \le n \le N_z)$, based on the expansions (4-10). For example, the condition $H_z(r_l^-, \theta, z_n) = H_z(r_l^+, \theta, z_n)$ can be written as

$$\begin{aligned} &\frac{1}{\mu^{(l-1)}(z_n)} \sum_{j=1}^{N_z} [\eta_j^{(l-1,e)}]^2 \phi_j^{(l-1,e)}(z_n) V_j^{(l-1,e)}(r_l, \theta) \\ &- \frac{1}{\mu^{(l)}(z_n)} \sum_{j=1}^{N_z} [\eta_j^{(l,e)}]^2 \phi_j^{(l,e)}(z_n) V_j^{(l,e)}(r_l, \theta) \\ &= H_z^{(l)}(r_l, \theta, z_n) - H_z^{(l-1)}(r_l, \theta, z_n). \end{aligned} \quad (13)$$

One equation in system (11) is obtained by considering the mth Fourier coefficient of the above.

The right hand side of Eq. (13) is related to the difference between the 1D solutions in S_l and S_{l-1}. Notice that the 1D solutions for regions S_l and S_{l-1} are different. Therefore, the right hand side of (13) is non-zero in general. The vector $\boldsymbol{c}_m$ can be written as

$$\boldsymbol{c}_m = \begin{bmatrix} \boldsymbol{c}_m^{(1)} \\ \boldsymbol{c}_m^{(2)} \\ \vdots \\ \boldsymbol{c}_m^{(L)} \end{bmatrix}, \quad \boldsymbol{c}_m^{(l)} = \begin{bmatrix} \boldsymbol{c}_m^{(l,1)} \\ \boldsymbol{c}_m^{(l,2)} \\ \boldsymbol{c}_m^{(l,3)} \\ \boldsymbol{c}_m^{(l,4)} \end{bmatrix}, \quad (14)$$

where the four blocks of $\boldsymbol{c}_m^{(l)}$ correspond to H_z, E_z, H_τ and E_τ, respectively. In particular, if

$$H_z^{(l)}(r_l, \theta, z_n) - H_z^{(l-1)}(r_l, \theta, z_n) = \sum_{m=-\infty}^{\infty} c_{m,n}^{(l,1)} e^{\mathrm{i}m\theta},$$

then $\boldsymbol{c}_m^{(l,1)}$ is the column vector for $c_{m,n}^{(l,1)}$, $n = 1, 2, ..., N_z$. The 2nd, 3rd and 4th blocks of $\boldsymbol{c}_m^{(l)}$ are related to $E_z^{(l)} - E_z^{(l-1)}$, $H_\tau^{(l)} - H_\tau^{(l-1)}$, $E_\tau^{(l)} - E_\tau^{(l-1)}$, respectively.

Inserting the cylindrical wave expansions of $V_j^{(l-1,e)}$ and $V_j^{(l,e)}$ into Eq. (13), the coefficients of $e^{\mathrm{i}m\theta}$ give rise

to an equation that links the unknowns $a_{j,m}^{(l-1,e)}$, $b_{j,m}^{(l-1,e)}$, $a_{j,m}^{(l,e)}$ and $b_{j,m}^{(l,e)}$ (for $1 \le j \le N_z$) to $c_{m,n}^{(l,1)}$. This equation corresponds to one row of Eq. (11), i.e., the row with the right hand side $c_{m,n}^{(l,1)}$. All N_z such equations (for $z = z_n$, $1 \le n \le N_z$) are put together and they correspond the block $\boldsymbol{c}_m^{(l,1)}$ in the right hand side of Eq. (11). Similar equations are established from the continuity of E_z, H_τ and E_τ at r_l and z_n, and these equations correspond to the rows of Eq. (11) where the right hand side elements are $c_{m,n}^{(l,2)}$, $c_{m,n}^{(l,3)}$ and $c_{m,n}^{(l,4)}$, respectively. At r_l, a total of $4N_z$ equations are obtained.

Notice that $\mathbf{A}_m$ is a banded matrix with a bandwidth of $O(N_z)$, therefore the system (11) can be solved in $O(LN_z^3)$ operations. Notice that the dependence on L is linear. In contrast, if the classical modal method is used, the coefficient matrix in the final linear system is essentially a full matrix and the required number of operations is proportional to L^3. Therefore, VMEM has a major advantage for bull's eye structures with many grooves.

For a normal incident plane wave, we assume the electric field is in the x direction, thus, $E_x^{(i)} \neq 0$, $H_y^{(i)} \neq 0$, and all other components are zero. The 1D solutions $\{\mathbf{E}^{(l)}, \mathbf{H}^{(l)}\}$ retain this property. The two nonzero components $E_x^{(l)}$ and $H_y^{(l)}$ depend only on the vertical variable z. Since the z components of the 1D solutions are zero, the first two blocks of $\boldsymbol{c}_m^{(l)}$ are zero. For the 3rd and 4th blocks, we notice that

$$H_\tau^{(l)}(r_l,\theta,z) - H_\tau^{(l-1)}(r_l,\theta,z) = \left[H_y^{(l)}(z) - H_y^{(l-1)}(z)\right]\cos\theta, \tag{15}$$

$$E_\tau^{(l)}(r_l,\theta,z) - E_\tau^{(l-1)}(r_l,\theta,z) = -\left[E_x^{(l)}(z) - E_x^{(l-1)}(z)\right]\sin\theta. \tag{16}$$

Therefore, the Fourier coefficients are nonzero only when $m = \pm 1$ [8]. This implies that $\boldsymbol{x}_m = \mathbf{0}$ if $m \neq \pm 1$, and we only have to solve Eq. (11) for $m = \pm 1$. In fact, we only have to solve the equation for $m = 1$, since the $\boldsymbol{x}_{-1}$ is related to $\boldsymbol{x}_1$. It can be verified that

$$a_{j,-1}^{(l,e)} = -a_{j,1}^{(l,e)}, \quad b_{j,-1}^{(l,e)} = -b_{j,1}^{(l,e)}, \tag{17}$$

$$a_{j,-1}^{(l,h)} = a_{j,1}^{(l,h)}, \; b_{j,-1}^{(l,h)} = b_{j,1}^{(l,e)}. \tag{18}$$

Therefore, expansions (8), (9) and (10) can be drastically simplified. As a result, H_z and E_z simply depend on θ as $\sin\theta$ and $\cos\theta$, respectively.

5. Numerical results

In this section, we apply the VMEM developed in the previous sections to analyze bull's eye structures in a gold film of thickness $D = 280\,\text{nm}$ for a normal incident wave with wavelength 800 nm. The refractive index of gold is assumed to be $n = 0.1808 + 5.117\text{i}$. The medium surrounding the film and in the hole is air. Yamada and Terakawa [11] proposed a near optimal bull's eye structure with three grooves, where the radius of the central hole is $r_1 = 200\,\text{nm}$, the inner radius of the first groove is $r_2 = 540\,\text{nm}$, the width, depth and period of the grooves are $w = 300\,\text{nm}$, $d = 90\,\text{nm}$ and $P = 780\,\text{nm}$, respectively. Using FDTD, Yamada and Terakawa [11] found a normalized transmission coefficient $T = 9.74$, where T is defined as the ratio between the total transmitted power and the power of the incident wave impinging on the hole. Using VMEM and $N_z = 166$ points to discretize z, we obtain $T = 9.7742$. The agreement with the result of [11] is quite good. Numerical convergence with respect to N_z has been observed. For $N_z = 94$, 118 and 142, we obtain $T = 9.795$, 9.778, 9.7747, respectively.

For the above bull's eye structure with three grooves, we investigate the influence of some key parameters on the normalized transmission coefficient. In Fig. 2(a) and 2(b), we show the dependence of T on the hole radius r_1 and the first groove inner radius r_2, respectively. It can be seen that T reaches local maxima at approximately $r_1 = 200\,\text{nm}$ and $r_2 = 540\,\text{nm}$, respectively. These results support the conclusion of [11] that the above bull's eye structure with three grooves is near optimal. Many authors have studied the influence of the inner radius of the first groove. We notice that our result shown Fig. 2(b) is quite similar to the experimental result of Carretero-Palacios *et al.* [7]. It is also quite similar to

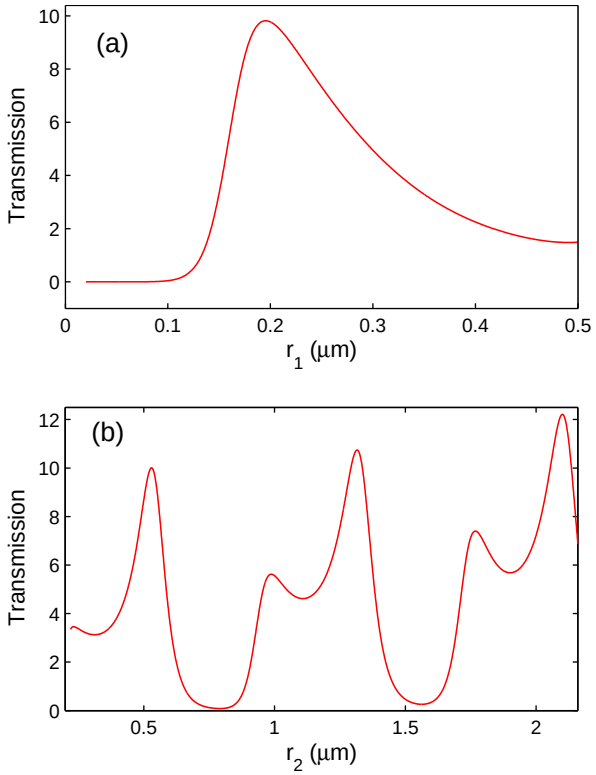

Fig. 2. Dependence of the normalized transmission coefficient T on, (a) hole radius r_1, (b) first groove inner radius r_2, for a bull's eye structure with three grooves.

the 2D result of Cui and He [23] for a slit-groove structure. For the 2D case, the local maxima appear to decrease as r_2 is increased [23], but for the 3D bull's eye structure, the local maxima appear to increase as r_2 is increased. Therefore, high transmission is still possible with only three grooves, if the grooves are put at some proper locations far away from the hole.

Next, we analyze the dependence of T on the number of grooves N_g. For a bull's eye structure with the parameters given above ($r_1 = 200\,\text{nm}$, $r_2 = 540\,\text{nm}$, $P = 780\,\text{nm}$, etc), we obtain the result shown in Fig. 3(a). Notice that a very high transmission can be achieved if

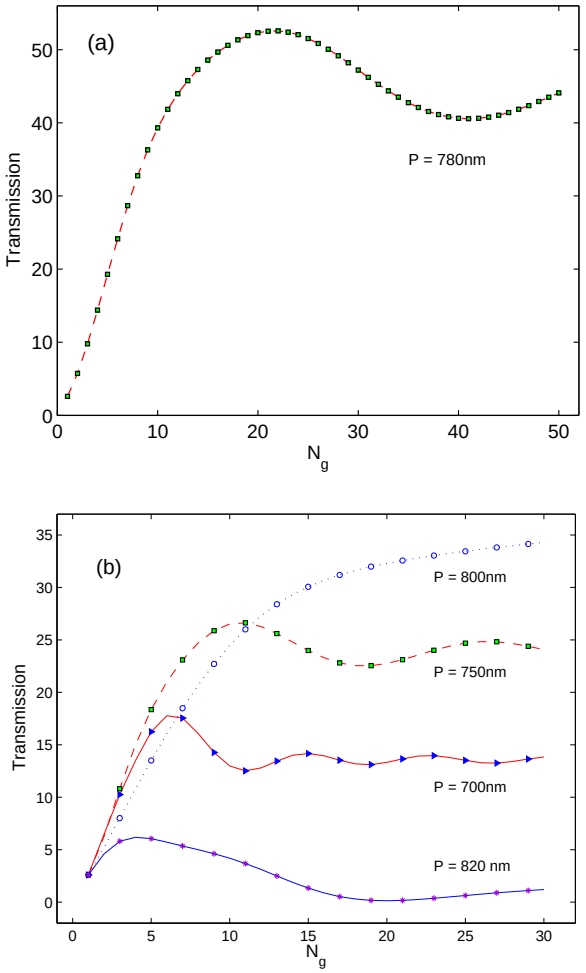

Fig. 3. Dependence of the normalized transmission coefficient on the number of grooves N_g for (a) $P = 780\,\text{nm}$, (b) $P = 700$, 750, 800 and 820 nm.

more grooves are used. In particular, T reaches a maximum about 52.56 for $N_g = 22$. The period $P = 780\,\text{nm}$ appears to be a good choice. In Fig. 3(b), we show the results for a few different values of P. Notice that a different vertical scale is used in Fig. 3(b). The normalized transmission T is less than 35 for all four values of P and for all $N_g \leq 30$.

Our method is efficient for bull's eye structures with many grooves. On an iMac with a 3.4 GHz CPU, the computation time for a few different values of N_g are listed in the following table:

N_g	1	2	3	30	50
Time (sec)	1.7	3.4	5.4	89	172

Table 1. Time required for analyzing bull's eye structures with N_g grooves.

6. Conclusion

The VMEM is a rigorous computational method for solving the frequency-domain Maxwell's equations. It is applicable to structures consisting of a number of regions where the material properties depend only on z. The method combines field expansions in 1D eigenmodes with a suitable method for solving 2D scalar Helmholtz equations. The special variant developed in this paper is suitable for rotationally symmetric structures with annular regions. The method is efficient because it solves the different Fourier modes (in θ) separately for a general incident wave, and solves only one Fourier mode for a normal incident plane wave. Using the newly developed VMEM, we analyzed some bull's eye structures in a gold film, and found a particular structure with 22 grooves for which the normalized transmission is greater than 52. Our method is very efficient and relatively simple to implement, and it should be useful in the design and optimization of rotationally symmetric photonic structures.

Acknowledgments

This work was partially supported by the Research Grants Council of Hong Kong Special Administrative Region, China, under project CityU 11301914.

References

[1] T. W. Ebbesen, H. L. Lezec, H. F. Ghaemi, T. Thio, and P. A. Wolff, "Extraordinary optical transmission through subwavelength hole arrays," Nature **391**, 667–669 (1998).

[2] C. Genet and T. W. Ebbesen, "Light in tiny holes," Nature **445**, 39–46 (2007).

[3] F. J. Garcia-Vidal, L. Martin-Moreno, T. W. Ebbesen, and L. K. Kuipers, "Light passing through subwavelength apertures," Rev. Mod. Phys. **82**, 729787 (2010).

[4] T. Thio, H. L. Lezec, T. W. Ebbesen, K. M. Pellerin, G. D. Lewen, A. Nahata, and R. A. Linke, "Giant optical transmission of subwavelength apertures: physics and applications," Nanotechnology **13**, 429–432 (2002).

[5] H. J. Lezec, A. Degiron, E. Devaux, R. A. Linke, L. Martín-Moreno, F. J. García-Vidal, and T. W. Ebbesen, "Beaming light from a subwavelength aperture," Science **297**, 820–822 (2002).

[6] H. Liu and P. Lalanne, "Microscopic theory of the extraordinary optical transmission," Nature **452**(7188), 728–731 (2008).

[7] S. Carretero-Palacios, O. Mahboub, F. J. Garcia-Vidal, L. Martin-Moreno, Sergio G. Rodrigo, C. Genet, and

T. W. Ebbesen, "Mechanisms for extraordinary optical transmission through bull's eye structures," Opt. Express **19**, 10429–10442 (2011).

[8] E. Popov, M. Neviére, A.-L. Fehrembach, and N. Bonod, "Optimization of plasmon excitation at structured apertures," Appl. Opt. **44**, 6141–6154 (2005).

[9] E. Popov, M. Neviére, A.-L. Fehrembach, and N. Bonod, "Enhanced transmission of light through a circularly structured aperture," Appl. Opt. **44**, 6898–6904 (2005).

[10] O. Mahboub, S. C. Palacios, C. Genet, F. J. Garcia-Vidal, S. G. Rodrigo, L. Martin-Moreno, and T. W. Ebbesen, "Optimization of bulls eye structures for transmission enhancement," Opt. Express **18**, 11292–11299 (2010).

[11] A. Yamada and M. Terakawa, "Reverse design of a bull's eye structure based on the plasmonic far-field pattern," Opt. Express **21**, 21273–21284 (2013).

[12] A. M. Kern and O. J. F. Martin, "Surface integral formulation for 3D simulations of plasmonic and high permittivity nanostructures," J. Opt. Soc. Am. A **26**, 732–740 (2009).

[13] L. Li, "New formulation of the Fourier modal method for crossed surface-relief gratings," J. Opt. Soc. Am. A **14**, 2758–2767 (1997).

[14] E. Silberstein, P. Lalanne, J.-P. Hugonin, and Q. Cao, "Use of grating theories in integrated optics," J. Opt. Soc. Am. A **18**, 2865–2875 (2001).

[15] G. Granet and J. P. Plumey, "Parametric formulation of the Fourier modal method for crossed surface-relief gratings," J. Opt. A **4**, S145–S149 (2002).

[16] V. Liu and S. Fan, "S^4: A free electromagnetic solver for layered periodic structures," Computer Physics Communications **183**, 2233–2244 (2012).

[17] X. Lu, H. Shi, and Y. Y. Lu, "Vertical mode expansion method for transmission of light through a single circular hole in a slab," J. Opt. Soc. Am. A **31**, 293–300 (2014).

[18] S. Boscolo and M. Midrio, "Three-dimensional multiple-scattering technique for the analysis of photonic-crystal slabs," J. Lightw. Technol. **22**, 2778–2786 (2004).

[19] L. Yuan and Y. Y. Lu, "Dirichlet-to-Neumann map method for analyzing hole arrays in a slab," J. Opt. Soc. Am. B **27**, 2568–2579 (2010).

[20] L. Yuan and Y. Y. Lu, "An efficient numerical method for analyzing photonic crystal slab waveguides," J. Opt. Soc. Am. B **28**, 2265–2270 (2011).

[21] H. Shi and Y. Y. Lu, "Vertical mode expansion method for analyzing elliptic cylindrical objects in a layered background," J. Opt. Soc. Am. A **32**, 630–636 (2015).

[22] H. Shi and Y. Y. Lu, "Efficient vertical mode expansion method for scattering by arbitrary layered cylindrical structures," Opt. Express **23**, 14618–14629 (2015).

[23] Y. Cui and S. He, "A theoretical re-examination of giant transmission of light through a metallic nano-slit surrounded with periodic grooves," Opt. Express **17**, 13995–14000 (2009).